SPECTRAL VARIATION BETWEEN SOUTH POLAR RESIDUAL ICE DEPOSITS IN MARS YEARS 28 AND 29. S. F. A. Cartwright[1], W. M. Calvin[1], and K. D. Seelos[2], [1]Dept. of Geological Sciences and Engineering, University of Nevada—Reno, 1664 N. Virginia St., MS 0172, Reno, NV 89557 (scartwright@nevada.unr.edu), [2]Johns Hopkins University Applied Physics Laboratory, 11100 Johns Hopkins Road, Laurel, MD 20723

Introduction: The south polar layered deposits (SLPD) of Mars constitute a ~4 km high dome of dusty water ice layers that have long been thought to represent a record of past climatic variation [1]. The portion of the SPLD that sits above an elevation of ~2 km retains a bright, meter to tens-of-meters deposit of CO_2 ice throughout the year (Fig 1). In addition to a number of unique erosional features on its surface [2], small exposures of water ice have been observed around the margins of the SPLD's CO_2 ice veneer, though it is unclear whether they constitute an uppermost layer of the SPLD or annealed seasonal water ice [3, 4]. Determining the detailed compositions and grain sizes of ice and dust mixtures that make up the upper portion of the SPLD may illuminate the formation mechanisms of those erosional features and, more broadly, the climate record of the SPLD.

The best equipped dataset to help constrain those attributes are the targeted observations of the Compact Reconnaissance Imaging Spectrometer for Mars (CRISM) [5], which has captured hundreds of hyperspectral visible-to-near-infrared observations of the SPLD at spatial resolutions up to 18 m/px. Here we use four such observations (Fig. 1, Table 1) to compare the distribution of CO_2 and water ice at early and late solar longitude (L_s) in Mars Years 28 and 29 in preparation for detailed spectral modeling of grain size and composition.

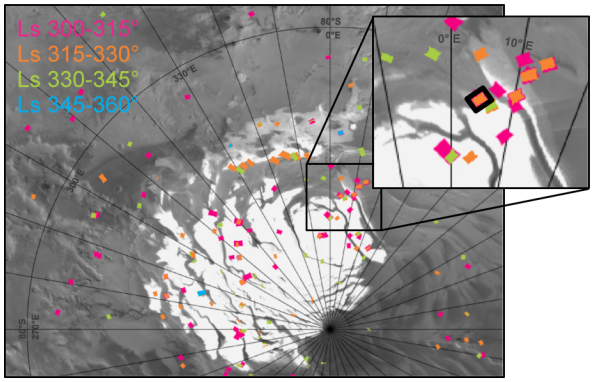

Figure 1: Mars Orbiter Camera (MOC) albedo map of the south polar region, overlaid with CRISM image footprints colored by L_s. The study region covered by observations in Table 1 is centered at 85.6° S, 6.3° E and outlined within the inset.

Table 1: Observational metadata for the four CRISM observations used in this work.

Observation	L_s (°)	Mars Year	Ref. Code
FRT00006EC9	288.82	28	E28
FRT00008354	330.68	28	L28
FRT00011936	227.06	29	E29
FRT00014639	321.78	29	L29

Methods: The four CRISM targeted observations were processed using the CRISM Analysis Toolkit (CAT) 7.4 plugin for Harris Geospatial ENVI 5.5 image analysis software [6]. Targeted Reduced Records (TRR3) downloaded from the Planetary Data System were converted to CAT file format before Lambertian photometric and volcano scan atmospheric corrections were applied. The resulting spectral cubes were then map-projected and georeferenced to FRT00006EC9 using 15 tie points distributed across the scene.

Due to its clear differentiation of several apparent units, FRT00008354 was used to define a collection of 33 regions of interest (ROIs) in and around the study region's residual CO_2 ice-covered mesas (Fig. 2). These ROIs capture dark and light portions of erosional pit floors and the light halos that surround them, different portions of the mesas themselves, and dark and light ice exposures elsewhere in the scene, including a reticulated debris field.

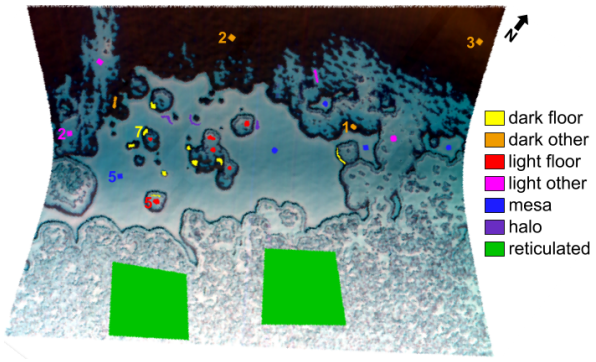

Figure 2: FRT00008354 (RGB = 2.52, 1.50, 1.07 μm) overlaid with ROIs color-coded by type. Note the flat mesas eroded into "swiss cheese terrain" by a number of pits. Numbers reference ROIs compared in Figure 3.

Averaged spectra of the ~20–50 pixels comprising each ROI were calculated for each of the four images, allowing for a direct comparison of spectral differences not only across distinct units in the study region, but also across two seasons in two Mars Years. These first-order evaluations of compositional difference will be used to guide further investigation with unmixing models by Kieffer and others [7, 8] that will constrain differences in grain size and dust/ice abundance.

Initial Results: *Inter-annual comparisons:* Averaged spectra for ROIs covering light pit floors, mesa tops, and other light exposures in late L_s observations show strong CO_2 ice signatures varying only in relative albedo (Fig. 3A), with a significant 10% increase being found in L29 (see Table 1 for corresponding observation ID for this and other reference codes). ROIs covering dark exposures outside the mesas in both late L_s observations show a marked difference in average spectra: while L28 shows a consistent strong water ice signature, in L29 those ROIs display varying degrees of apparent water ice with CO_2 (Fig. 3B).

Intra-annual comparisons: ROIs for light pit floors show elevated water ice content compared to early L_s observations in each year, as evidenced by broadening of the absorption at 1.5 μm. Similarly, there is a pronounced difference between dark exposures in early and late L_s, with dark exposures in pit floors and elsewhere shifting from strong CO_2 ice signatures in E28 to water ice in L28 (Fig 3C).

ROI spectra in mesa tops show greater depth of CO_2 absorption features compared to ROIs capturing the higher albedo halos that surround erosional pits, indicating a possible difference in grain size. Spectral signatures of the large ROIs covering the reticulated debris field in the lower portion of the study region (Fig. 2) indicate slight differences in water content between early and late L_s in both years.

Discussion: The observed intra-annual differences between early and late L_s observations are as expected: seasonal CO_2 frost present in southern spring obscures water ice signatures that may be visible by the time frost has been removed in late southern summer (e.g., Fig. 3C). This frost cover is expected to persist up to L_s = 320–340°, meaning the observed inter-annual differences between L28 and L29 (Fig. 3A, B) may hint at processes shifting that cutoff, such as enhanced removal following the MY 28 dust storm and/or increased deposition during the winter of MY 29 [9, 10]. Comparison of spectral modeling results across additional study areas and L_s values (Fig. 1) will help constrain the thickness and yearly retreat of seasonal CO_2 ice, allowing the nature of underlying water ice deposits to be more accurately characterized.

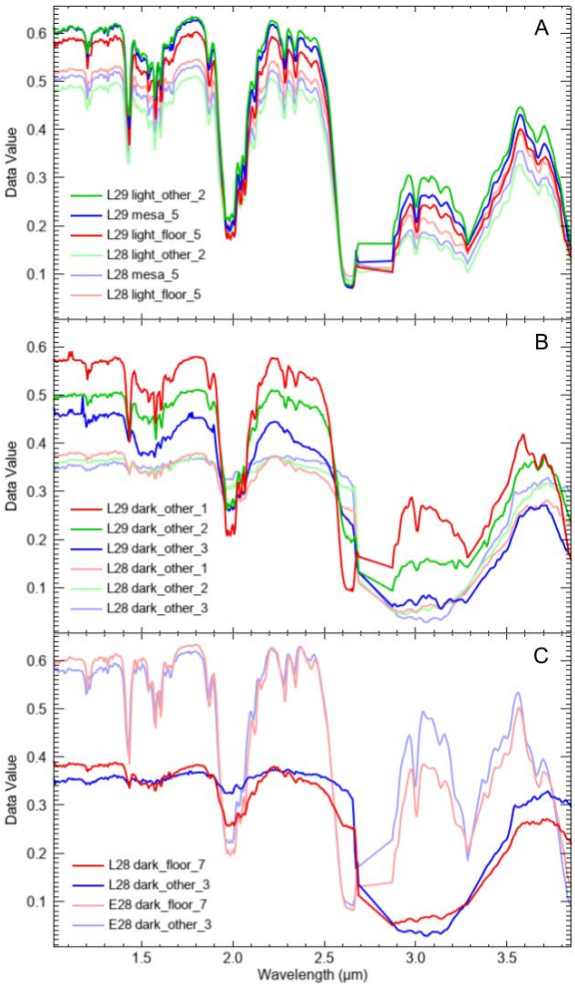

Figure 3: Plots of averaged ROI spectra showing comparisons between A) various light-toned exposures in late L_s observations for MY 28 and 29, B) dark exposures outside mesas in late L_s observations for MY 28 and 29, and C) dark pit floors in mesa interiors and dark exposures elsewhere in early and late L_s for MY 28. Line color links ROIs while opacity differentiates timeframes. See Table 1 for observation IDs corresponding to shorthand reference codes and Figure 2 for the location of numbered ROIs.

References: [1] Byrne (2009) *Annu. Rev. Earth Planet. Sci., 37,* 535–560. [2] Thomas et al. (2009) *Icarus, 203,* 352–375. [3] Douté et al. (2007) *Plan. & Space Sci., 55,* 113–133. [4] Montmessin et al. (2007) *JGR, 112,* E08S17. [5] Murchie et al. (2007) *JGR, 112,* E05S03. [6] Morgan et al. (2009) https://pds-geosciences.wustl.edu/missions/mro/CRISM_Workshop_090322_CAT_MFM.pdf [7] Kieffer et al. (2000) *JGR, 105,* 9653–9699. [8] Lapotre el al. (2017) *JGR, 122,* 983–1009. [9] Calvin et al. (2017) *Icarus, 292,* 144–153. [10] Piqueux et al. (2015) Icarus, 251, 164–180.